Flexural modes of graphene resonators derived from the reactive empirical bond-order potential

Yisen Wang ⬤ and Liang Huang[*]

Institute of Computational Physics and Complex Systems and Key Laboratory for Magnetism and Magnetic Materials of MOE,
Lanzhou University, Lanzhou, Gansu 730000, China

Flexural modes play an important role in mechanical, thermal, and electronic properties of two-dimensional materials. Graphene nanoelectromechanical systems have been found in wide applications and have attracted huge attention recently, where the molecular dynamics (MD) simulation has been an essential route for the investigation of the mechanical responses of the system. In this paper, based on the expressions and parameters of the reactive empirical bond-order potential for the carbon-carbon atomic interactions implemented in Large-scale Atomic/Molecular Massively Parallel Simulator, the linearized part of the force for each atom along the z direction has been obtained, yielding the stiffness matrix of the graphene lattice. By diagonalizing the stiffness matrix, the flexural modes and their corresponding frequencies can be obtained. The results have been validated with MD simulations in circular and square graphene resonators with different sizes. Since the stiffness matrix for graphene resonators with arbitrary shapes can be obtained readily from our results, we expect broad applications where eigenfrequencies and flexural modes are needed in the analysis for the nanoscale resonators.

I. INTRODUCTION

Graphene is a monolayer of carbon atoms tightly packed in a two-dimensional (2D) honeycomb lattice that has been extensively investigated [1–13] since its discovery in 2004 [1,2]. Due to its peculiar mechanical and electronic properties [6–9], graphene has been considered as an excellent candidate for the nanoelectromechanical (NEM) resonators [14–18]. The graphene resonators are made from suspended single- or multilayered graphene sheets, and can be actuated either optically or electrically [19]. The advantages of the nanometer scale graphene resonators are unambiguous, e.g., extremely small size, low power consumption, and ultrafast speed, which leads to broad applications such as ultrasensitive sensors [20–22], Berry phase switches [23], and so on. Recently, ultrasmall accelerometers were fabricated with suspended double-layer graphene ribbons with attached silicon proof mass, whose size is at least two orders of magnitude smaller than the conventional state-of-the-art silicon ones [24,25].

For 2D materials, the surface-to-volume ratio is much larger than that for bulk materials, which is also the case for the ratio of the number of surface phonon modes to the total number of all the phonon modes. For one-atom-thick 2D material, the surface phonon modes are the only choice as all the atoms are immersed in the surface [26]. In this sense, the out-of-plane flexural modes, belonging to the surface phonon modes, play an important role in the mechanical [27], thermal [28–31], and electronic properties [32] of the graphene NEM resonators, as the out-of-plane motion is their most dominant dynamics [19,27–29,32]. In fact, the nonlinear interactions between flexural modes is a fundamental intrinsic dissipation

mechanism, and sets the upper limit of the quality factor (Q factor), which is one of the most important parameters for NEM resonators [27]. The flexural phonon modes also make a dominant contribution to the thermal conductivity of graphene, which has been confirmed by recent experiments and numerical simulations [28,29]. In addition, due to the out-of-plane deformation and the pseudomagnetic field effect, the strained nanobubbles in graphene sheet can be exploited to confine the electrons, and affect the charge transport behaviors in the NEM resonators [32–34].

The flexural modes and other mechanical properties of graphene resonators have been investigated with different methods, such as continuum plate theory [35–37], lattice structure method [38,39], and molecular mechanics method [40,41]. For the method of continuum plate theory, the graphene sheet is modeled as a 2D plate, and the dynamics of the plate is described by a partial differential equation, whose parameters are obtained directly from the experimental results or calculated from the empirical potentials of graphene. Comparing with molecular dynamics (MD) simulation, this method needs less computational resources and is suitable for large systems [35–37]. For the lattice structure method, the carbon atoms are regarded as nodes with concentrated atomic mass, linked by covalent bonds which are modeled as an equivalent structural beams with axial, bending, and torsional capability [38,39]. The elastic parameters of the beams can be calculated with the Odegard approach [42]. The results given by these two methods are in good agreement with each other [38]. The molecular mechanics method is also widely used in the investigation of the graphene resonators. In 2010, Sadeghi *et al.* introduced a hybrid atomistic-structural element method in the shape of a hexagonal lattice consisting of six neighbors for each carbon atom, whose equations of motion are derived using Hamilton's principle [40]. A similar method,

---

[*]huangl@lzu.edu.cn

the atomistic finite element method, has also been proposed in the investigation of mechanical properties of 2D materials, where the carbon-carbon bond was approximated with shear bending and axial stretching beam, and the parameters of the beam were derived from an empirical potential. By using this method, the nonlinear frequency response of a single-layered graphene sheet was computed by the commercial finite element code ANSYS [41].

Advances in fabrication techniques enable the production of the nanodevice with a few thousand atoms. For example, a mass sensing experiment with a resolution of 1.7 yg (1 yg = 10^{-24} g) has been reported with a carbon nanotube of length ~150 nm, which contains only ~30 thousand carbon atoms in total [43]. Undoubtedly, the MD method is capable to investigate the mechanical properties of such devices with the same parameters and environment as in the experiments, where the empirical potential is the core in the MD simulations. The reactive empirical bond-order (REBO) potential has been widely used in the numerical simulations of graphene resonators as it can give an accurate description for the bond-bond interaction, bond breaking, and bond reforming [44–46]. In fact, many MD simulations were performed with the REBO potential in Large-scale Atomic/Molecular Massively Parallel Simulator (LAMMPS), which has been a very popular setup in the literature [47–49]. Therefore, it is important to obtain the flexural modes of graphene nanoresonators employing the REBO potential for the carbon-carbon atomic interactions based on the expression and parameters implemented in the LAMMPS.

In this work, the theory of small oscillations (TSOs) has been used to derive the flexural modes directly from REBO potentials [50]. We treat the carbon atoms as mass points which move in the force field given by the REBO potential. The simplified expression of the potential is given in Sec. II. Note that this expression is the same as the original one as some functions are constants under the small oscillation assumption, i.e., when the distance between adjacent carbon atoms is less than 1.7 Å. The linear part of the force along the z direction is derived from this simplified expression, which implies that the fourth-nearest neighbor must be taken into account. Then the stiffness matrix will be derived in Sec. III with the expression of the force and the neighbor list of the graphene sheet, where the flexural modes and their corresponding frequencies are given by the eigenvectors and eigenvalues of the stiffness matrix, respectively. In Sec. IV, it is shown that these results match with the MD simulation very well, and also agree with the prediction of Kirchhoff's plate theory. Finally, a short summary and discussion is given in Sec. V. It should be stressed that although the flexural modes can be obtained from other methods, our approach can be more accurate and in the meantime can obtain the fundamental frequencies and the corresponding flexural modes for large systems that are comparable to the state-of-the-art experiments. Furthermore, our results of the expression of the stiffness matrix are general and can be used to the graphene resonators with arbitrary geometry, and the method in deriving the expression of the stiffness matrix can also be expanded to deal with other 2D materials taking into account of their specific empirical potentials.

TABLE I. The parameter values in Eq. (2).

Parameter	CC	CH	HH
Q_{ij} (Å)	0.313 460	0.340 776	0.370 471
α_{ij} (Å^{-1})	4.746 5391	4.102 549 8	3.536 298 6
A_{ij} (eV)	10 953.544	149.940 99	32.817 356
$B_{ij}^{(1)}$ (eV)	12 388.792	32.355 187	29.632 593
$B_{ij}^{(2)}$ (eV)	17.567 065		
$B_{ij}^{(3)}$ (eV)	30.714 932		
$\beta_{ij}^{(1)}$ (Å^{-1})	4.720 452 3	1.434 458 1	1.715 892 2
$\beta_{ij}^{(2)}$ (Å^{-1})	1.433 213 2		
$\beta_{ij}^{(3)}$ (Å^{-1})	1.382 691 3		

II. REBO POTENTIAL

Without external field, the graphene sheet is a conservative system, whose potential energy is a function of position only. At low temperature, the carbon atoms oscillate about the equilibrium configuration, which is one of the stable equilibrium positions. For such a system, the dynamics is completely determined by the potential energy after the initial condition is specified. When the total energy or the vibration amplitude is small, it can be described effectively by the TSO. In the following, we shall first briefly recall the REBO potential, which is an energy function for the solid carbon and hydrocarbon molecules that is based on an empirical bond order formalism [44–46]

$$E^{\text{REBO}} = \frac{1}{2} \sum_i \sum_{j \neq i} \left[V_{ij}^{\text{R}} + b_{ij} V_{ij}^{\text{A}} \right], \quad (1)$$

where

$$V_{ij}^{\text{R}} = w_{ij}(r_{ij}) \left[1 + \frac{Q_{ij}}{r_{ij}} \right] A_{ij} e^{-\alpha_{ij} r_{ij}},$$

$$V_{ij}^{\text{A}} = -w_{ij}(r_{ij}) \sum_{n=1}^{3} B_{ij}^{(n)} e^{-\beta_{ij}^{(n)} r_{ij}}, \quad (2)$$

and

$$b_{ij} = \frac{1}{2} \left[p_{ij}^{\sigma\pi} + p_{ji}^{\sigma\pi} \right] + \pi_{ij}^{\text{rc}} + \pi_{ij}^{\text{dh}}. \quad (3)$$

V_{ij}^{R} and V_{ij}^{A} are repulsive and attractive pairwise potentials between atom i and j, and b_{ij} is the bond order term. The parameter values in Eq. (2) are given in Table I.

The b_{ij}s are roughly equivalent to the usual chemical concept of the bond order, which takes into account of a variety of chemical effects that affect the strength of the covalent bonding interaction, such as coordination numbers, bond angles, and dihedral angles. The expressions of the terms that contribute to b_{ij} are given by

$$p_{ij}^{\sigma\pi} = \left[1 + \sum_{k \neq i,j} w_{ik}(r_{ik}) g_i(\cos\theta_{jik}) e^{\lambda_{jik}} \right.$$

$$\left. + P_{ij}(N_{ij}^C, N_{ij}^H) \right]^{-1/2} \quad (4)$$
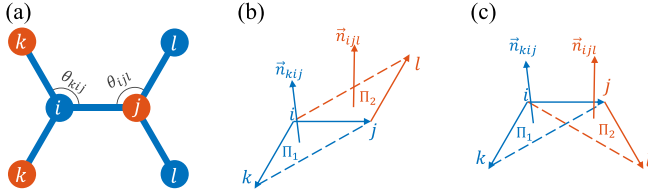
FIG. 1. (a) The bond angles which are used as the variables in angle penalty function $g_i(\cos\theta_{jik})$. (b), (c) The definition of torsion angles. There are two kinds of torsion angles: (b) atom k and atom l are on the different sides of the bond r_{ij}; (c) atom k and atom l are on the same side of the bond r_{ij}.

and

$$\pi_{ij}^{dh} = T_{ij}(N_{ij}, N_{ji}, N_{ij}^{conj}) \sum_{k\neq i,j} \sum_{l\neq i,j} (1 - \cos^2\omega_{kijl})$$
$$\times w'_{ik}(r_{ik}) w'_{jl}(r_{jl}) \Theta[\sin(\theta_{jik}) - s^{min}]$$
$$\times \Theta[\sin(\theta_{ijl}) - s^{min}], \qquad (5)$$

where the summations indices k and l are indicated in Fig. 1. The term π_{ij}^{rc} is a three-dimensional cubic spline in the variables $(N_{ij}, N_{ji}, N_{ij}^{conj})$, which describes the contributions to the bond order from radical and conjugation effects. In Eqs. (1)–(5), $w_{ij}(r_{ij})$ and $w'_{ij}(r_{ij})$ are bond weight terms, which can give a good description for the smooth transition from bonded to nonbonded interaction between atoms i and j [46], $g_i(x)$ is the angle penalty function, N_{ij}, N_{ji}, and N_{ij}^{conj} are the coordination numbers, $P_{ij}(N_{ij}^C, N_{ij}^H)$, $\pi_{ij}^{rc}(N_{ij}, N_{ji}, N_{ij}^{conj})$, and $T_{ij}(N_{ij}, N_{ji}, N_{ij}^{conj})$ are the functions of the coordination numbers, and $\Theta(x)$ is the Heaviside step function, i.e., $\Theta(x) = 1$ for $x > 0$, and $\Theta(x) = 0$ otherwise. It should be noted that there are some discrepancies among different versions of the potential [44–46]. In order to compare the results given by the TSO with that of the MD simulations, the expressions and parameters implemented in the 16 Mar 2018 version of LAMMPS are chosen in this work.

On the hypothesis of small oscillations, the carbon atoms in the graphene sheet undergo infinitesimal displacements with respect to their equilibrium positions. Under such a condition, some functions in the REBO potential are constants: (a) the bond weight terms $w_{ij}(r_{ij})$ and $w'_{ij}(r_{ij})$ are always 1 when the bond length between adjacent atoms is smaller than 1.7 Å [46] (the equilibrium bond length is 1.397 Å for graphene); (b) the Heaviside step function $\Theta(x)$ in Eq. (5) is 1 when the bond angles are in the range of (5.7392°, 174.2608°) (the equilibrium bond angle is 120°); (c) the coordination numbers N_{ij}^C, N_{ij}^H, N_{ij}, N_{ji}, N_{ij}^{conj} are 2, 0, 2, 2, 9, respectively, and keep constant during the MD simulations, which results in that the values of the functions $P_{ij}(N_{ij}^C, N_{ij}^H)$, $\pi_{ij}^{rc}(N_{ij}, N_{ji}, N_{ij}^{conj})$, $T_{ij}(N_{ij}, N_{ji}, N_{ij}^{conj})$ are also constants (Table II). Besides that, the $e^{\lambda_{jik}}$ term is used for improving the potential-energy surface for abstraction of hydrogen atoms from hydrocarbons. As a result, the value of $e^{\lambda_{jik}}$ is 1 for the pure graphene sheet which only contains carbon atoms [45,46].

TABLE II. The values of functions of the coordination numbers.

Function	Value
$P_{CC}(2, 0)$	$-0.027\,603$
$\pi_{CC}^{rc}(2, 2, 9)$	0
$T_{CC}(2, 2, 9)$	$-0.004\,048$

The angle penalty function $g_i(\cos\theta_{jik})$ is a fifth-order piecewise spline, which switches smoothly between a form $g_C^{(1)}$ that is appropriate for covalent compounds with low coordination numbers and another form $g_C^{(2)}$ which is suitable for highly coordinated bulk materials,

$$g_C(\cos\theta_{jik}) = g_C^{(1)}(\cos\theta_{jik}) + S'[t_N(N_{ij})]$$
$$\times [g_C^{(2)}(\cos\theta_{jik}) - g_C^{(1)}(\cos\theta_{jik})]. \qquad (6)$$

For the graphene sheet which vibrates around the equilibrium position, the value of $S'[t_N(N_{ij})]$ is one and the $g_C(\cos\theta_{jik})$ is equal to $g_C^{(2)}(\cos\theta_{jik})$. The interpolation points for $g_C^{(2)}(\cos\theta_{jik})$ for graphene sheets are listed in Table III.

In short, based on the hypothesis of small oscillations, the REBO potential for the graphene sheet can be written as

$$E^{REBO} = \frac{1}{2} \sum_i \sum_{j\in i's\ NN} [V_{ij}^R + b_{ij} V_{ij}^A], \qquad (7)$$

where "NN" represents nearest neighbor, and

$$V_{ij}^R = \left[1 + \frac{Q_{ij}}{r_{ij}}\right] A_{ij} e^{-\alpha_{ij} r_{ij}},$$

$$V_{ij}^A = -\sum_{n=1}^{3} B_{ij}^{(n)} e^{-\beta_{ij}^{(n)} r_{ij}}, \qquad (8)$$

$$b_{ij} = \frac{1}{2}[p_{ij}^{\sigma\pi} + p_{ji}^{\sigma\pi}] + \pi_{ij}^{dh}$$

$$= \frac{1}{2}\left[0.972\,397 + \sum_{k\neq i,j} g_i(\cos\theta_{jik})\right]^{-1/2}$$

$$+ \frac{1}{2}\left[0.972\,397 + \sum_{l\neq i,j} g_i(\cos\theta_{ijl})\right]^{-1/2}$$

$$- 0.004\,048 \sum_{k\neq i,j}\sum_{l\neq i,j} \sin^2\omega_{kijl}. \qquad (9)$$

TABLE III. Interpolation points for the quintic spline $g_C^{(2)}(\cos\theta_{jik})$.

$\cos\theta$	g_i	$\partial g_i/\partial(\cos\theta)$	$\partial^2 g_i/\partial(\cos\theta)^2$
-1	$-0.010\,000$	$0.104\,000$	$0.000\,000$
$-\frac{2}{3}$	$0.028\,207$	$0.131\,443$	$0.140\,229$
$-\frac{1}{2}$	$0.052\,804$	$0.170\,000$	$0.370\,000$
$-\frac{1}{3}$	$0.097\,321$	$0.400\,000$	$1.980\,00$
1	$8.000\,000$	20.2436	43.9336

Note that this reduced form of the REBO potential is the same as the original one given by Eqs. (1)–(5) when the bond length and bond angle undulate around the equilibrium value.

III. STIFFNESS MATRIX

The core step of the TSO is to construct the stiffness matrix V [50]. Here we consider a graphene sheet which contains N carbon atoms with fixed boundary condition. To address the effect of flexural modes, we only consider the out-of-plane (z-direction) motion, which, according to the TSO, can be described as the superposition of the flexural modes when the deviation of the system from the stable equilibrium condition is small enough. In this case, the REBO potential can be expanded around the equilibrium position

$$E^{\text{REBO}}(\mathbf{z}) = E_0 + \sum_i \left.\frac{\partial E^{\text{REBO}}}{\partial z_i}\right|_{\mathbf{z}=0} z_i + \frac{1}{2}\sum_{i,j}\left.\frac{\partial^2 E^{\text{REBO}}}{\partial z_i \partial z_j}\right|_{\mathbf{z}=0} z_i z_j + \cdots, \quad (10)$$

where $\mathbf{z} = [z_1, \ldots, z_N]$ are the displacements of the carbon atoms from their equilibrium positions in the z direction, and E_0 is the potential energy of the equilibrium position. The coefficients of the second term in the series, e.g., $\partial E^{\text{REBO}}/\partial z_i$, vanish automatically as $\mathbf{z} = 0$ gives the equilibrium position. The coefficients of the quadratic term give exactly the stiffness matrix $V = [V_{ij}]_{N \times N}$, where

$$V_{ij} = -\frac{\partial^2 E^{\text{REBO}}}{\partial z_i \partial z_j} = \partial F_{z_i}/\partial z_j, \quad (11)$$

and $F_{z_i} = -\partial E^{\text{REBO}}/\partial z_i$ is the force acting on the ith atom due to the REBO potential.

Suppose that $E_{ij} = V_{ij}^{\text{R}} + b_{ij}V_{ij}^{\text{A}}$ is the bond energy between atom i and j, the terms which contain z_i in Eq. (7) can be written as

$$E_i = \sum_j E_{ij} + \sum_{j,p} E_{jp}, \quad (12)$$

where the summations over j and p are indicated in Fig. 2. In this sense, we have

$$F_{z_i} = -\frac{\partial E_i}{\partial z_i}$$
$$= -\sum_j \left[\frac{\partial V_{ij}^{\text{R}}}{\partial r_{ij}} + b_{ij}\frac{\partial V_{ij}^{\text{A}}}{\partial r_{ij}}\right]\frac{\partial r_{ij}}{\partial z_i}$$
$$- \sum_j \left[V_{ij}^{\text{A}}\frac{\partial b_{ij}}{\partial z_i} + \sum_{p\in j\text{'s NN}} V_{jp}^{\text{A}}\frac{\partial b_{jp}}{\partial z_i}\right]$$
$$= F_{z_i}^{\text{RA}} + F_{z_i}^b, \quad (13)$$

where $F_{z_i}^{\text{RA}}$ and $F_{z_i}^b$ are the forces induced by the variation of bond length and bond order, respectively.

$F_{z_i}^{\text{RA}}$ is derived from the terms of repulsive and attractive pairwise potentials between atom i and atom j by assuming that all the bond angles and torsion angles in graphene are at the equilibrium values, whose expression can be expanded into Taylor series around the equilibrium distance

$r_0 = 1.39768$ Å between two neighboring atoms:

$$F_{z_i}^{\text{RA}} = \sum_{j\in i\text{'s NN}}\left[\frac{a_2}{r_0^2}(z_j - z_i)^3 + \frac{3a_3}{4r_0^3}(z_j - z_i)^5 + \cdots\right]. \quad (14)$$

It is clear that the force $F_{z_i}^{\text{RA}}$ is nonlinear and can be neglected in the small displacement situation. The detailed derivation can be found in Sec. 1 of the Appendix.

Substituting Eq. (9) into Eq. (13), we have

$$F_{z_i}^b = -\sum_j \left\{V_{ij}^{\text{A}}\left[\frac{1}{2}\left(\frac{\partial p_{ij}^{\sigma\pi}}{\partial z_i} + \frac{\partial p_{ji}^{\sigma\pi}}{\partial z_i}\right) + \frac{\partial \pi_{ij}^{\text{dh}}}{\partial z_i}\right]\right.$$
$$\left. + \sum_{p\in j\text{'s NN}} V_{jp}^{\text{A}}\left[\frac{1}{2}\left(\frac{\partial p_{jp}^{\sigma\pi}}{\partial z_i} + \frac{\partial p_{pj}^{\sigma\pi}}{\partial z_i}\right) + \frac{\partial \pi_{jp}^{\text{dh}}}{\partial z_i}\right]\right\}, \quad (15)$$

where

$$\frac{\partial p_{ij}^{\sigma\pi}}{\partial z_i} \simeq -\frac{0.07594}{r_0^2}\sum_k\left(3z_i - \frac{3}{2}z_j - \frac{3}{2}z_k\right),$$
$$\frac{\partial p_{ji}^{\sigma\pi}}{\partial z_i} \simeq -\frac{0.07594}{r_0^2}\sum_l\left(\frac{1}{2}z_i - \frac{3}{2}z_j + z_l\right),$$
$$\frac{\partial p_{jp}^{\sigma\pi}}{\partial z_i} \simeq -\frac{0.07594}{r_0^2}\left(\frac{1}{2}z_i + z_p - \frac{3}{2}z_j\right),$$
$$\frac{\partial p_{pj}^{\sigma\pi}}{\partial z_i} = 0,$$
$$\frac{\partial \pi_{ij}^{\text{dh}}}{\partial z_i} \simeq -\frac{0.021589}{r_0^2}\left(3z_i - z_j - \sum_k z_k\right),$$
$$\frac{\partial \pi_{jp}^{\text{dh}}}{\partial z_i} \simeq \frac{0.005397}{r_0^2}(6z_j - 2z_p - 4z_i), \quad (16)$$

and the summations over k and l are indicated in Fig. 1. Equations (15) and (16) imply that the force derived from the bond order term is linear, thus the bond angle effect and the dihedral angle effect in the bond order term are two physical origins for the bending stiffness of the graphene sheet. The detailed derivation of $p_{ij(jp)}^{\sigma\pi}$ and $\pi_{ij(jp)}^{\text{dh}}$ can be found in Secs. 2 and 3 of the Appendix, respectively.

Substitute Eqs. (15) and (16) into Eq. (13), the linear part of the force F_{z_i} can be written as

$$F_i = c_i z_i + c_j \sum_j z_j + c_p \sum_p z_p + c_q \sum_q z_q + c_s \sum_s z_s, \quad (17)$$

where the values of c_i, c_j, c_p, c_q, c_s can be found in the caption of Fig. 2. Note that due to the strong nonlinear effects in the REBO potential, e.g., $F_{z_m}^{\text{RA}}$, this expression is valid only when the displacement is small. With Eqs. (11) and (17), the elements of the stiffness matrix can be constructed by the following expression:

$$V_{mn} = \begin{cases} c_i, & n = m, \\ c_j, & n = m\text{'s 1st NN}, \\ c_p, & n = m\text{'s 2nd NN}, \\ c_q, & n = m\text{'s 3rd NN}, \\ c_s, & n = m\text{'s 4th NN}, \\ 0, & \text{otherwise}. \end{cases} \quad (18)$$
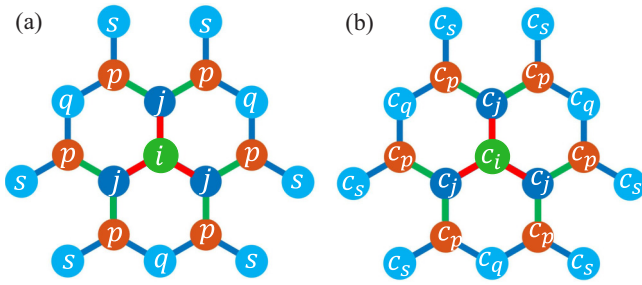
FIG. 2. (a) The neighbors of the ith atom in the REBO potential. (b) The parameters in Eq. (17), where c_i, c_j, c_p, c_q, c_s are -265.0031, 126.2128, -92.6734, $4.192\,44$, $-2.096\,22$ J/m^2, respectively.

The flexural modes and the corresponding eigenfrequencies can be calculated numerically by solving the eigenequation

$$V\varphi_i = \lambda_i \varphi_i, \tag{19}$$

where $\{\lambda_i, \varphi_i, i = 1, \dots, N\}$ is the set of eigenvalues and eigenvectors of V. Then, φ_i will be the ith flexural mode of the graphene sheet with eigenfrequency $\omega_i = \sqrt{-\lambda_i/m_0}$, where m_0 is the mass of a carbon atom. It should be noted that Eq. (18) is quite general thus the construction of the stiffness matrix for resonators with different shapes is straightforward.

IV. FLEXURAL MODES AND SCALING OF THE FUNDAMENTAL FREQUENCY OF GRAPHENE RESONATORS

As examples, this formalism has been applied to investigate the flexural modes of circular and square graphene resonators, as defined in Fig. 3, where coordinates and the neighbor list of all the carbon atoms can be easily obtained. The boundary layers (red empty circles) are chosen so that up to the fourth-nearest neighbors of the inner atoms (blue full circles) near the boundary are fixed during the MD simulations. The inner atoms can move in the force field derived by the REBO potential. In reality, the interactions between graphene and the substrate or other materials is characterized by adhesion energy, which stems from the van
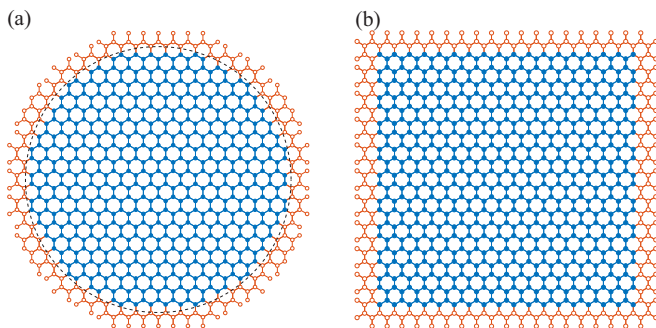

FIG. 3. The setup of circular (a) and square (b) graphene resonators. During the MD simulations, the red atoms close to the boundary are fixed, and the inner blue atoms are movable. The boundary layers (red empty circles) are chosen so that up to the fourth-nearest neighbors of the inner atoms (blue full circles) near the boundary are motionless.
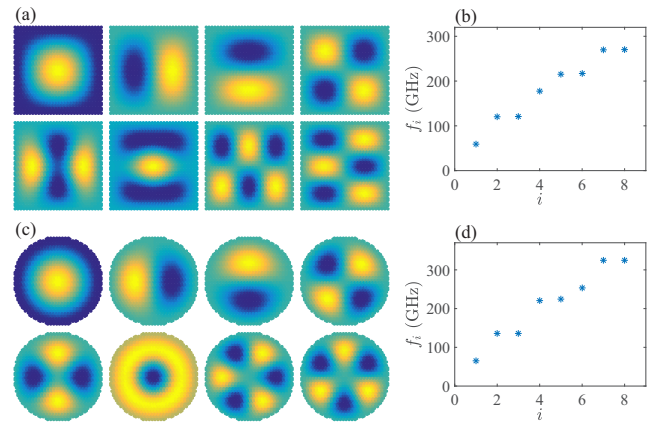

FIG. 4. The vibration morphology of the first eight flexural modes (a), (c) and their corresponding eigenfrequencies (b), (d) for the circular (a), (b) and square (c), (d) graphene resonators. $f_i = \omega_i/2\pi$. Light gray (yellow) and black (dark blue) in the morphology plots indicate maximum and minimum values of the flexural modes, respectively.

der Waals forces or chemical bond between graphene and the substrate [51]. When the amplitude of the vibration is small, the graphene resonators can be strongly clamped to the substrate and the rigid boundary condition is appropriate [52].

The stiffness matrix of the graphene resonators can be obtained straightforwardly with Eq. (18) and the neighbor list of the carbon atoms. The flexural modes and their corresponding frequencies can be calculated numerically by solving the eigenproblem Eq. (19). Figure 4 shows the vibration morphology of the first eight flexural modes and their corresponding eigenfrequencies for the circular and square graphene resonators. In this figure, the diameter and side length of the resonators are 7.24 and 7.01 nm, respectively.

In order to validate the TSO approach, the eigenfrequency of the first flexural mode for the circular and square graphene resonators with different sizes has been calculated with both the TSO and the MD simulations using the LAMMPS package. The REBO potential is used to model the covalent bonds between carbon atoms. Verlet algorithm is employed to integrate the Newton's equations of motion, and the time step is set as 1.0 fs. All the carbon atoms are initially placed at their equilibrium positions, and after an energy minimization of the system, the graphene resonators are fixed at their boundary layers as shown in Fig. 3. The whole system is then equilibrated at a specific temperature (1.0 K) for 100 ps with canonical ensemble by using Nosé-Hoover thermostat. Then the thermostat is removed, and the graphene resonators are actuated by assigning an initial velocity profile along the z direction obtained from the first flexural mode without any modification of the position of the carbon atoms [27]. Thereafter, all the carbon atoms move freely in the microcanonical ensemble for 10 ns, and the positions of all the carbon atoms are collected every ten time steps for further analyses.

The key parameter for the MD simulations is the kinetic energy fed into the system. Due to the existence of nonlinearity, the resonance frequency of the graphene resonator is dependent on the amplitude of vibration. As a result, the initial velocity is set in such a way that the largest relative
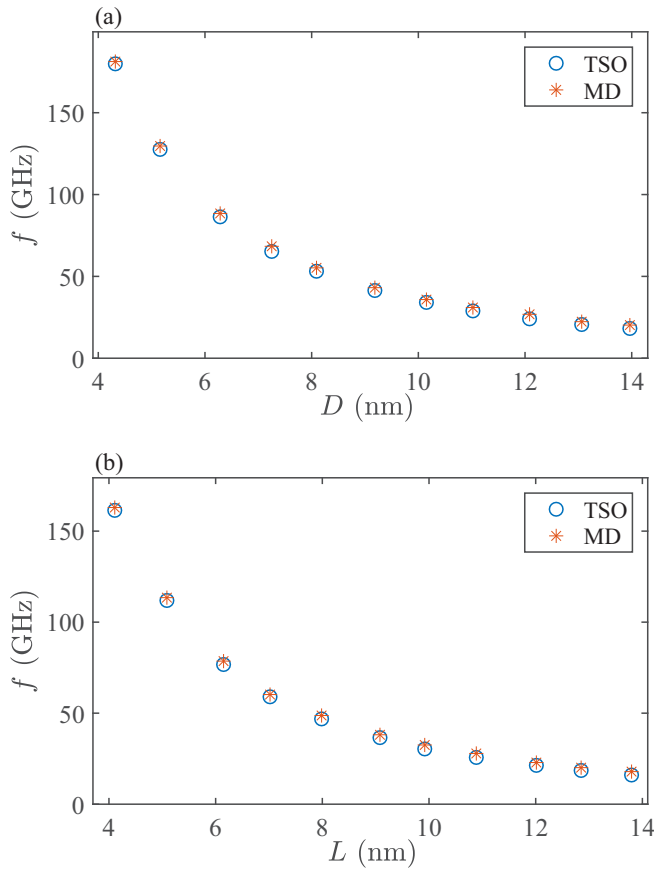
FIG. 5. The resonance frequencies of the first flexural mode for the circular (a) and square (b) graphene resonators with different sizes. The blue circles and the red asterisks represent the frequencies that are estimated with the TSO method and the MD simulations, respectively.

deformations η are approximately equal for all the resonators with different sizes during the MD simulations, which is defined as the ratio of the amplitude of vibration in the z direction to the size of the graphene resonators. In order to minimize the nonlinear effect, the relative deformation η is set at around 0.005.

Figure 5 shows the resonance frequencies for the first flexural mode for the circular and square graphene resonators with different sizes. The blue circles are estimated with the TSO method, i.e., the eigenfrequency of the first mode of the stiffness matrix [Eq. (19)], and the red asterisks are the result of the MD simulations, which are obtained by applying fast Fourier transform (FFT) to the trajectory of the center of the mass of the graphene resonators. It can be seen that the TSO values of the linear model match the ones estimated with MD simulations very well, and the resonance frequency decreases as the size of the graphene resonator increases. Note that, on one hand, an energy minimization has been performed before the MD simulations, and the in-plane stress has been relaxed. On the other hand, the displacements of the carbon atoms are very small, and the nonlinear effects can be ignored. Therefore, the resonant frequency is entirely determined by the bending rigidity that is originated from the bond angle effect and torsional angle effect of the REBO potential. Under these
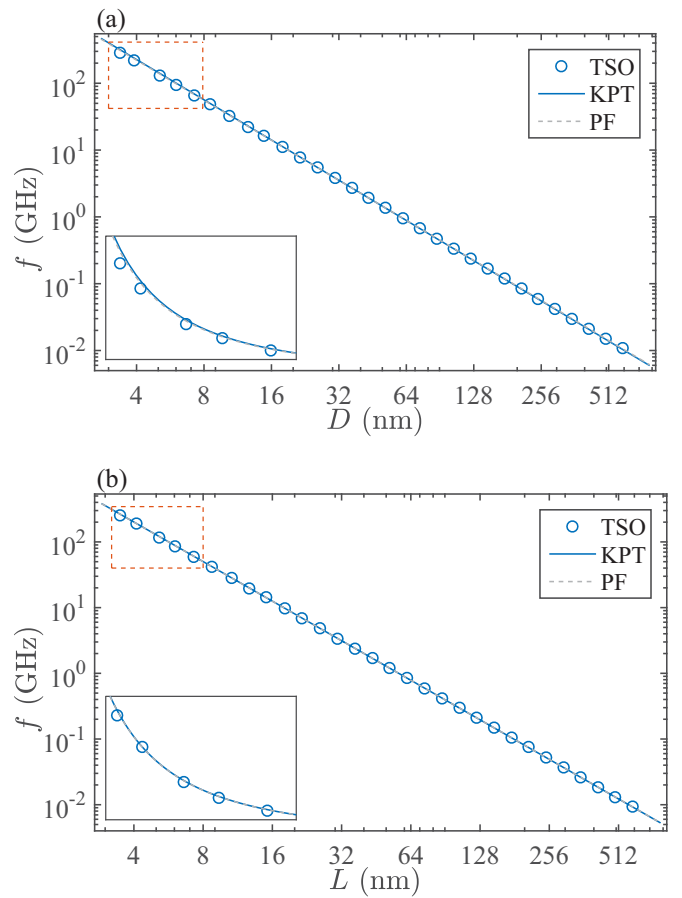
FIG. 6. The loglog plot of the resonance frequencies of the first flexural mode (blue circles) obtained from the stiffness matrix Eq. (18) for the circular (a) and square (b) graphene resonators with different sizes. The blue solid lines are fitted with the Kirchhoff's plate theory (KPT) Eq. (21), the gray dashed lines are fitted with the power fitting Eq. (22). The size of the graphene resonators ranges from 4 nm (624 carbon atoms) to 600 nm (13 million carbon atoms). The inset in each plot shows the zoom-in region in the linear scale indicated by red dashed rectangles. Note that, when the system size is large, the inverse iteration method [53] on sparse matrix has been applied to solve the resonance frequency of the flexural modes.

conditions, the dynamics of the resonators can be described by Kirchhoff's plate theory, that the fundamental frequency of the clamped circular plate is given by the following relation:

$$ f = 2.06\pi \sqrt{\frac{B}{m_p}} \frac{1}{D^2}, \tag{20} $$

where B is bending rigidity, m_p is the mass per unit area, and D is the diameter of the plate [54]. For graphene, the value of m_p is 7.865×10^{-7} kg/m^2, which is calculated by considering the mass of 1.99×10^{-26} kg for a single carbon atom. Figure 6(a) shows the resonance frequencies of the first flexural mode for the circular graphene resonators in the log-log scale. The blue circles are the theoretical values obtained from the stiffness matrix by the inverse-iteration method, while the solid blue line is the fitting curve with

$$ f = \frac{a}{D^2}, \tag{21} $$

and the value of a is 3.52×10^{-6} m^2/s. Comparing Eq. (21) with Eq. (20), we can get the value of the bending rigidity B from these data, which is 1.45 eV. This value is very close to the one deduced also from the REBO potential by calculating the second derivative of the strain energy density with respect to the curvature [55] and the experimental one [56], which are 1.4 and 1.44 eV, respectively. Figure 6(b) shows the results for square graphene resonators, which also agree with Kirchhoff's plate theory well. Note that we here mainly focus on the first flexural mode, the other eigenvalues and eigenvectors can also been calculated by the inverse iteration method, where the detailed procedure can be found in Ref. [53]. Experimentally, the first few vibration modes are imperative due to the easy excitation of these modes. The Arnoldi based scheme can also be employed to obtain the first few eigenvalues of the stiffness matrix [57,58].

In addition, it has been proposed in Ref. [40] that for double clamped graphene resonators, the resonance frequency f of the first flexural mode scales with the size L as

$$f = \frac{a}{L^b} \tag{22}$$

and it was found that the value of b is 2.09 [40], which is a little different from the Kirchhoff's plate theory of 2 [Eq. (20)]. We have also performed power fitting (PF) with the TSO data and the values of b are 1.991 and 1.999 for the circular and square resonators, respectively. This fitting is depicted in Fig. 6 by the light gray dashed lines. It can be seen that the KPT fitting and the PF almost coincide with each other, that from the fitting, it is difficult to distinguish which one agrees with the data better. However, from Fig. 6(a), when the system's size is small, the data deviate from both of the fitting curves, where the data are a little bit below the curves [inset of Fig. 6(a)]. This is in agreement with the limitations of the KPT that it is only valid for plates where its size is much larger than the thickness. Since the graphene is only one atom thick, only when it is large enough will it follow the KPT. From Fig. 6(a), the critical size is around 16 nm for the circular graphene resonator. However, for square graphene resonators, the data fit with the KPT well, and also the PF yields a scaling component of 1.999, which is quite close to 2.

The dynamical behaviors of graphene resonators can be affected by various factors. Typically the suspended graphene sheets will appear under stress, which will change the effective spring constant of the system [19]. This stress can be tuned by a DC gate voltage [19], or by changing the temperature due to the thermal expansion and contraction of the metal electrodes [59]. The electron-phonon coupling may also have an effect on the dynamics of the resonators. It can be tuned by doping and biaxial tensile strain, and usually it is very weak when the strain is small for the pristine graphene [60]. However, Castro *et al.* showed that the flexural phonons are a major source of electron-phonon scattering in suspended graphene especially when the temperature is higher than 10 K [61]. In this sense, this is an interesting question that may need further investigation. In addition, the defect, suspension distance to the trench, air friction, etc., can also affect the dynamics of the resonators.

V. CONCLUSION AND DISCUSSION

In this paper, the flexural modes for graphene resonators have been derived directly from the REBO potential in LAMMPS for carbon-carbon atomic interactions. First, since small oscillation and thus linear responses are needed, the reduced expression of the REBO potential with small oscillation assumption has been obtained, and the z-component linearized force for each atom has been derived. Second, based on the expression of the z-component force, the stiffness matrix elements for an atom have been obtained, thus the whole stiffness matrix for the graphene resonator can be constructed given the neighbor list of all the carbon atoms. Note that for graphene resonators with different shapes, only the elements for the boundary atoms need to be treated separately, thus the construction of the whole stiffness matrix can be made readily regardless of the specific shapes. Third, the flexural modes are nothing but the eigenvectors of the stiffness matrix, and their eigenfrequencies can be read out from the corresponding eigenvalues. For large systems, diagonalization of the stiffness matrix to yield all the flexural modes may be unrealistic, but the inverse iteration method can be employed to calculate the flexural modes and their frequencies efficiently. Indeed, the largest graphene resonator that we have calculated has a length of 600 nm, with 13 million carbon atoms in total.

As examples, we have calculated the flexural modes and frequencies of the circular and square graphene resonators with different sizes. In order to validate these results, the MD simulations have been performed on the same resonators when the system size is small, which indicates that the resonance frequencies estimated with MD simulations match the theoretical ones estimated from the TSO method very well. These results have also been fitted with Kirchhoff's plate theory, showing an excellent agreement. From the fitting, it is found that the value of the bending rigidity is 1.45 eV, which is very close to the values reported in the literature.

Since the stiffness matrix for graphene resonators with arbitrary shapes can be obtained readily from our results, we expect broad applications where eigenfrequencies and flexural modes are needed in the analysis for the resonators. This method is general and is applicable not only to the graphene resonators with different shapes, but also to nanoelectromechanical devices based on other 2D materials with their particular expressions and parameter values of the empirical atomic potential, which could find broad applications in both physics and engineering.

APPENDIX: DERIVATION OF THE FORCE

The force acting on the ith atom in the z direction can be written as

$$F_{z_i} = F_{z_i}^{\mathrm{RA}} + F_{z_i}^{b}, \tag{A1}$$

where $F_{z_i}^{RA}$ and $F_{z_i}^b$ are the forces induced by the variation of bond length and bond order, respectively. The bond length force $F_{z_i}^{RA}$ is given by

$$F_{z_i}^{RA} = -\sum_j \left[\frac{\partial V_{ij}^R}{\partial r_{ij}} + b_{ij} \frac{\partial V_{ij}^A}{\partial r_{ij}} \right] \frac{\partial r_{ij}}{\partial z_i}, \qquad (A2)$$

and the bond order force $F_{z_i}^b$ can be written as

$$F_{z_i}^b = -\sum_j \left[V_{ij}^A \frac{\partial b_{ij}}{\partial z_i} + \sum_{p \in j\text{'s NN}} V_{jp}^A \frac{\partial b_{jp}}{\partial z_i} \right], \qquad (A3)$$

where

$$b_{ij(jp)} = \tfrac{1}{2}[p_{ij(jp)} + p_{ji(pj)}] + \pi_{ij(jp)}^{dh} \qquad (A4)$$

and the summation indices j and p are indicated in Fig. 2. The first two terms and the third term in Eq. (A4) are related with the bond angles between adjacent bonds and the torsional angles, respectively.

1. Bond length force

In order to calculate the bond length force $F_{z_i}^{RA}$, the equilibrium bond length r_0 should be estimated accurately in the first place. For this purpose, the bond order b_{ij} is regarded as a constant by assuming that all the bond angles and torsional angles in graphene are in their equilibrium positions. Then r_0 can be calculated by

$$\frac{\partial E_{ij}}{\partial r_{ij}} = 0, \qquad (A5)$$

where $E_{ij} = V_{ij}^R + b_{ij} V_{ij}^A$ is the bond energy between atoms i and j. The value of r_0 is approximately 1.397 68 Å, which has been validated by performing an energy minimization of graphene sheet in LAMMPS.

Expanding E_{ij} about r_0, we obtain

$$E_{ij} = a_0 + a_1(r_{ij} - r_0) + a_2(r_{ij} - r_0)^2 + a_3(r_{ij} - r_0)^3 + \cdots, \qquad (A6)$$

where a_0, a_1, a_2, and a_3 are -5.204, 0.000, 23.5191, and -61.0589, respectively. Substituting Eq. (A6) into Eq. (A2), we have

$$F_{z_i}^{RA} \simeq -\sum_j [2a_2(r_{ij} - r_0) + 3a_3(r_{ij} - r_0)^2] \frac{\partial r_{ij}}{\partial z_i}$$

$$\simeq \sum_j \frac{a_2}{r_0^2}(z_j - z_i)^3 + \frac{3a_3}{4r_0^3}(z_j - z_i)^5 + \cdots, \qquad (A7)$$

where $r_{ij} = \sqrt{r_0^2 + (z_j - z_i)^2}$ is taken as the bond length by assuming that the atoms are constrained in the equilibrium position in the x and y directions. Obviously, the bond length force contains only nonlinear terms, which implies that it has no effect on the bending rigidity.

2. Bond angle part of the bond order force

Now we consider the bond order force which is linear with respect to the z component of the displacements. It has two parts, the bond angle part and the torsion angle

part. Figure 1(a) shows the bond angles in graphene lattice. The $p_{ij}^{\sigma\pi}$ and $p_{ji}^{\sigma\pi}$ are related with bond angles θ_{jik} and θ_{ijl}, respectively. The derivative of the first term in Eq. (A4) can be written as

$$\frac{\partial p_{ij}^{\sigma\pi}}{\partial z_m} = \sum_k \frac{\partial p_{ij}^{\sigma\pi}}{\partial g_i(\cos\theta_{jik})} \frac{\partial g_i(\cos\theta_{jik})}{\partial \cos\theta_{jik}} \frac{\partial \cos\theta_{jik}}{\partial z_m}$$

$$= -\frac{1}{2} \sum_k \left[0.9724 + \sum_{k \neq i,j} g_i(\cos\theta_{jik}) \right]^{-3/2}$$

$$\times \frac{\partial g_i(\cos\theta_{jik})}{\partial \cos\theta_{jik}} \frac{\partial \cos\theta_{jik}}{\partial z_m}, \qquad (A8)$$

where $m = i, j, k$, and the summation index k runs over all the atoms marked by "k" in Fig. 1(a). For the graphene sheet, on the hypothesis of small oscillations along the z direction, all the bond angles θ_{jik} are approximately equal to $\frac{2}{3}\pi$. Substituting the values in Table III into Eq. (A8), we have

$$\frac{\partial p_{ij}^{\sigma\pi}}{\partial z_m} = -0.075\,94 \sum_k \frac{\partial \cos\theta_{jik}}{\partial z_m}, \qquad (A9)$$

where

$$\cos\theta_{jik} = \frac{\mathbf{r}_{ij} \cdot \mathbf{r}_{ik}}{|\mathbf{r}_{ij}||\mathbf{r}_{ik}|}. \qquad (A10)$$

If the atoms are constrained in the equilibrium position in the x and y directions, $\cos\theta_{jik}$ can be written as

$$\cos\theta_{jik} = \frac{-\frac{1}{2}r_0^2 + (z_i - z_j)(z_i - z_k)}{\sqrt{r_0^2 + (z_i - z_j)^2}\sqrt{r_0^2 + (z_i - z_k)^2}}. \qquad (A11)$$

The derivative of $\cos\theta_{jik}$ can be written as

$$\frac{\partial \cos\theta_{jik}}{\partial z_i} = \frac{2z_i - z_j - z_k}{\sqrt{r_0^2 + (z_i - z_j)^2}\sqrt{r_0^2 + (z_i - z_k)^2}}$$

$$- \cos\theta_{jik} \left[\frac{z_i - z_j}{r_0^2 + (z_i - z^j)^2} + \frac{z_i - z_k}{r_0^2 + (z_i - z^k)^2} \right], \qquad (A12)$$

$$\frac{\partial \cos\theta_{jik}}{\partial z_j} = \frac{z_i - z_k}{\sqrt{r_0^2 + (z_i - z_j)^2}\sqrt{r_0^2 + (z_i - z_k)^2}}$$

$$- \cos\theta_{jik} \left[\frac{z_j - z_i}{r_0^2 + (z_i - z^j)^2} \right], \qquad (A13)$$

and

$$\frac{\partial \cos\theta_{jik}}{\partial z_k} = \frac{z_i - z_j}{\sqrt{r_0^2 + (z_i - z_j)^2}\sqrt{r_0^2 + (z_i - z_k)^2}}$$

$$- \cos\theta_{jik} \left[\frac{z_k - z_i}{r_0^2 + (z_i - z^j)^2} \right]. \qquad (A14)$$

On the hypothesis of small oscillations along the z direction, $|z_i - z_j| \ll r_0^2$ and $\theta_{jik} \simeq \frac{2}{3}\pi$. As a result, we have

$$
\frac{\partial p_{ij}^{\sigma\pi}}{\partial z_m} \simeq
\begin{cases}
-\frac{0.075\,94}{r_0^2} \sum_k \left(3z_m - \frac{3}{2}z_j - \frac{3}{2}z_k\right), & m = i, \\[2mm]
-\frac{0.075\,94}{r_0^2} \sum_k \left(\frac{1}{2}z_m + z_k - \frac{3}{2}z_i\right), & m = j, \\[2mm]
-\frac{0.075\,94}{r_0^2} \left(\frac{1}{2}z_m + z_j - \frac{3}{2}z_i\right), & m = k.
\end{cases}
\tag{A15}
$$

A similar derivation process can be applied to the bond angles θ_{ijl},

$$
\frac{\partial p_{ji}^{\sigma\pi}}{\partial z_m} \simeq
\begin{cases}
-\frac{0.075\,94}{r_0^2} \sum_l \left(\frac{1}{2}z_m + z_l - \frac{3}{2}z_j\right), & m = i, \\[2mm]
-\frac{0.075\,94}{r_0^2} \sum_l \left(3z_m - \frac{3}{2}z_i - \frac{3}{2}z_l\right), & m = j, \\[2mm]
-\frac{0.075\,94}{r_0^2} \left(\frac{1}{2}z_m + z_i - \frac{3}{2}z_j\right), & m = l,
\end{cases}
\tag{A16}
$$

where the summation runs over all the atoms l in Fig. 1(a). It is clear that the force derived from the bond angle terms is linear with respect to the displacement, and is one of the most important contributions of the bending stiffness.

3. Torsion angle part of the bond order force

The torsion angle ω_{kijl} is the angle between the planes defined by the vectors $\mathbf{r}_{ik}$ and $\mathbf{r}_{ij}$, denoted by Π_1, and that defined by $\mathbf{r}_{ij}$ and $\mathbf{r}_{jl}$, denoted by Π_2. In Figs. 1(b) and 1(c), $\vec{n}_{kij}$ and $\vec{n}_{ijl}$ are the unit normal vectors of the planes Π_1 and Π_2, respectively. The $\vec{n}_{kij}$ and $\vec{n}_{ijl}$ are defined as

$$
\vec{n}_{kij} = \frac{\mathbf{r}_{ji} \times \mathbf{r}_{ik}}{|\mathbf{r}_{ji} \times \mathbf{r}_{ik}|},
$$

and

$$
\vec{n}_{ijl} = \frac{\mathbf{r}_{ij} \times \mathbf{r}_{jl}}{|\mathbf{r}_{ij} \times \mathbf{r}_{jl}|},
$$

respectively. The torsion angle ω_{kijl} is just the angle between the vectors $\vec{n}_{kij}$ and $\vec{n}_{ijl}$. On the hypothesis of small oscillations, we have $|\mathbf{r}_{ji} \times \mathbf{r}_{ik}| = |\mathbf{r}_{ij} \times \mathbf{r}_{jl}| \simeq \frac{\sqrt{3}}{2}r_0^2$.

As shown in Figs. 1(b) and 1(c), there are two kinds of torsion angles. For the torsion angle of Fig. 1(b), the expression of $\sin \omega_{kijl}$ can be written as

$$
\sin \omega_{kijl} \simeq |\Delta\vec{n}| = |\vec{n}_{ijl} - \vec{n}_{kij}|
$$
$$
= \frac{2\sqrt{3}}{3r_0^2} |\mathbf{r}_{ij}||\mathbf{r}_{jl} + \mathbf{r}_{ik}| \sin\langle \mathbf{r}_{ij}, \mathbf{r}_{jl} + \mathbf{r}_{ik}\rangle, \tag{A17}
$$

where $|\mathbf{r}_{ij}| \simeq r_0$, $\mathbf{r}_{jl} + \mathbf{r}_{ik} \simeq (z_k + z_l - z_i - z_j)\vec{z}$, and $\sin\langle \mathbf{r}_{ij}, \mathbf{r}_{jl} + \mathbf{r}_{ik}\rangle \simeq 1$ as $\mathbf{r}_{ij}$ is approximately perpendicular to $\mathbf{r}_{jl} + \mathbf{r}_{ik}$. As a result, we have

$$
\sin \omega_{kijl} = \frac{2\sqrt{3}}{3r_0} |z_i + z_j - z_k + z_l|. \tag{A18}
$$

Similarly, for Fig. 1(c), we have

$$
\sin \omega_{kijl} = \frac{2\sqrt{3}}{3r_0} |2z_i - 2z_j - z_k + z_l|. \tag{A19}
$$

The derivative of π_{ij}^{dh} is given by

$$
\frac{\partial \pi_{ij}^{\mathrm{dh}}}{\partial z_m} = T_e \sum_{k \neq i, j} \sum_{l \neq i, j} \frac{\partial \sin^2 \omega_{kijl}}{\partial z_m}, \tag{A20}
$$

where $m = i, j, k, l$. Substituting Eqs. (A18) and (A19) into Eq. (A20), we have

$$
\frac{\partial \pi_{ij}^{\mathrm{dh}}}{\partial z_m} =
\begin{cases}
\frac{16T_e}{3r_0^2} \left(3z_m - z_j - \sum_k z_k\right), & m = i, \\[2mm]
-\frac{16T_e}{3r_0^2} \left(z_i - 3z_m + \sum_l z_l\right), & m = j, \\[2mm]
-\frac{4T_e}{3r_0^2} \left(6z_i - 2z_j - 4z_m\right), & m = k, \\[2mm]
\frac{4T_e}{3r_0^2} \left(2z_i - 6z_j - 4z_m\right), & m = l,
\end{cases}
\tag{A21}
$$

where the summation indices k and l run over all the atoms k and l in Figs. 1(b) and 1(c), respectively. As a result, this force is also linear, and the dihedral angle's effect is another important contribution of the bending stiffness.

[1] K. S. Novoselov, A. K. Geim, S. V. Morozov, D. Jiang, Y. Zhang, S. V. Dubonos, I. V. Grigorieva, and A. A. Firsov, Science **306**, 666 (2004).

[2] C. Berger, Z. M. Song., T. B. Li., X. B. Li, A. Y. Ogbazghi, R. F. Z. T. Dai, A. N. Marchenkov, E. H. Conrad, P. N. First, and W. A. de Heer, J. Phys. Chem. B **108**, 19912 (2004).

[3] K. S. Novoselov, A. K. Geim, S. V. Morozov, D. Jiang, M. I. Katsnelson, I. V. Grigorieva, S. V. Dubonos, and A. A. Firsov, Nature (London) **438**, 197 (2005).

[4] D. Rodrigo, O. Limaj, D. Janner, D. Etezadi, F. J. García de Abajo, V. Pruneri, and H. Altug, Science **349**, 165 (2015).

[5] C. Lee, X. Wei, J. W. Kysar, and J. Hone, Science **321**, 385 (2008).

[6] C. W. J. Beenakker, Rev. Mod. Phys. **80**, 1337 (2008).

[7] A. H. Castro Neto, F. Guinea, N. M. R. Peres, K. S. Novoselov, and A. K. Geim, Rev. Mod. Phys. **81**, 109 (2009).

[8] N. M. R. Peres, Rev. Mod. Phys. **82**, 2673 (2010).

[9] S. Das Sarma, S. Adam, E. H. Hwang, and E. Rossi, Rev. Mod. Phys. **83**, 407 (2011).

[10] T. Higuchi, C. Heide, K. Ullmann, H. B. Weber, and P. Hommelhoff, Nature (London) **550**, 224 (2017).

[11] K. Zhou, K. S. Vasu, C. T. Cherian, M. Neekamal, J. Zhang, H. Ghorbanfekrkalashami, K. Huang, O. P. Marshall, V. G. Kravets, J. Abraham *et al.*, Nature (London) **559**, 236 (2018).

[12] A. P. Kauling, A. T. Seefeldt, D. P. Pisoni, R. C. Pradeep, R. Bentini, R. V. B. De Oliveira, K. S. Novoselov, and A. H. C. Neto, Adv. Mater. **30**, 1803784 (2018).

[13] Y. He, R. Hu, Y. Zhong, X. Zhao, Q. Chen, and H. Zhu, Nano Res. **11**, 1928 (2018).

[14] C. Chen, S. Rosenblatt, K. I. Bolotin, W. Kalb, P. Kim, I. Kymissis, H. L. Stormer, T. F. Heinz, and J. Hone, Nat. Nanotechnol. **4**, 861 (2009).

[15] K. Eom, H. S. Park, D. S. Yoon, and T. Kwon, Phys. Rep. **503**, 115 (2011).

[16] M. Poot and H. S. van der Zant, Phys. Rep. **511**, 273 (2012).

[17] D. J. Rizzo, G. Veber, T. Cao, C. Bronner, T. Chen, F. Zhao, H. Rodriguez, S. G. Louie, M. F. Crommie, and F. R. Fischer, Nature (London) **560**, 204 (2018).

[18] L. Tian, Nat. Commun. **9**, 383 (2018).

[19] J. S. Bunch, A. M. van der Zande, S. S. Verbridge, I. W. Frank, D. M. Tanenbaum, J. M. Parpia, H. G. Craighead, and P. L. McEuen, Science **315**, 490 (2007).

[20] A. Sakhaee-Pour, M. T. Ahmadian, and A. Vafai, Solid State Commun. **145**, 168 (2008).

[21] P. Weber, J. Güttinger, A. Noury, J. Vergaracruz, and A. Bachtold, Nat. Commun. **7**, 12496 (2016).

[22] P. Suvarnaphaet and S. Pechprasarn, Sensors **17**, 2161 (2017).

[23] F. Ghahari, D. Walkup, C. Gutierrez, J. F. Rodriguieznieva, Y. Zhao, J. Wyrick, F. D. Natterer, W. G. Cullen, K. Watanabe, T. Taniguchi *et al.*, Science **356**, 845 (2017).

[24] X. Fan, F. Forsberg, A. D. Smith, S. Schröder, S. Wagner, H. Rödjegård, A. C. Fischer, M. Östling, M. C. Lemme, and F. Niklaus, Nat. Electron. **2**, 394 (2019).

[25] X. Fan, F. Forsberg, A. D. Smith, S. Schröder, S. Wagner, M. Östling, M. C. Lemme, and F. Niklaus, Nano Lett. **19**, 6788 (2019).

[26] J.-W. Jiang, B.-S. Wang, J.-S. Wang, and H. S. Park, J. Phys.: Condens. Matter **27**, 083001 (2015).

[27] D. Midtvedt, A. Croy, A. Isacsson, Z. Qi, and H. S. Park, Phys. Rev. Lett. **112**, 145503 (2014).

[28] J. H. Seol, I. Jo, A. L. Moore, L. Lindsay, Z. H. Aitken, M. T. Pettes, X. Li, Z. Yao, R. Huang, D. Broido *et al.*, Science **328**, 213 (2010).

[29] L. Lindsay, D. A. Broido, and N. Mingo, Phys. Rev. B **82**, 115427 (2010).

[30] Y. Wang, Z. Zhu, Y. Zhang, and L. Huang, Appl. Phys. Lett. **112**, 111910 (2018).

[31] Y. Wang, Z. Zhu, Y. Zhang, and L. Huang, Phys. Rev. E **97**, 012143 (2018).

[32] N. N. Klimov, S. Jung, S. Zhu, T. Li, C. A. Wright, S. D. Solares, D. B. Newell, N. B. Zhitenev, and J. A. Stroscio, Science **336**, 1557 (2012).

[33] B. Amorim, A. Cortijo, F. De Juan, A. G. Grushin, F. Guinea, A. Gutierrezrubio, H. Ochoa, V. Parente, R. Roldan, P. Sanjose *et al.*, Phys. Rep. **617**, 1 (2016).

[34] M. Xu, Y. Wang, R. Bao, L. Huang, and Y.-C. Lai, Europhys. Lett. **114**, 47006 (2016).

[35] J. Atalaya, A. Isacsson, and J. M. Kinaret, Nano Lett. **8**, 4196 (2008).

[36] S. Jiang, S. Shi, and X. Wang, J. Phys. D: Appl. Phys. **47**, 045104 (2014).

[37] J. R. Mianroodi, S. A. Niaki, R. Naghdabadi, and M. Asghari, Nanotechnology **22**, 305703 (2011).

[38] S. Arghavan and A. V. Singh, J. Appl. Phys. **110**, 084308 (2011).

[39] A. Sakhaeepour, M. T. Ahmadian, and R. Naghdabadi, Nanotechnology **19**, 085702 (2008).

[40] M. Sadeghi and R. Naghdabadi, Nanotechnology **21**, 105705 (2010).

[41] S. O. Gajbhiye and S. P. Singh, J. Phys. D: Appl. Phys. **48**, 145305 (2015).

[42] M. O. Gregory, S. G. Thomas, M. N. Lee, and E. W. Kristopher, Compos. Sci. Technol. **62**, 1869 (2002).

[43] J. Moser, J. Guttinger, A. Eichler, M. J. Esplandiu, D. E. Liu, M. I. Dykman, and A. Bachtold, Nat. Nanotechnol. **8**, 493 (2013).

[44] D. W. Brenner, Phys. Rev. B **42**, 9458 (1990).

[45] D. W. Brenner, O. A. Shenderova, J. A. Harrison, S. J. Stuart, B. Ni, and S. B. Sinnott, J. Phys.: Condens. Matter **14**, 783 (2002).

[46] S. J. Stuart, A. B. Tutein, and J. A. Harrison, J. Chem. Phys. **112**, 6472 (2000).

[47] J. Hu, X. Ruan, and Y. P. Chen, Nano Lett. **9**, 2730 (2009).

[48] S. Chen, Q. Wu, C. Mishra, J. Kang, H. Zhang, K. Cho, W. Cai, A. A. Balandin, and R. S. Ruoff, Nat. Mater. **11**, 203 (2012).

[49] Q. Pei, Y. Zhang, and V. B. Shenoy, Carbon **48**, 898 (2010).

[50] H. Goldstein, C. Poole, and J. Safko, *Classical Mechanics*, 3rd ed. (Addison Wesley, San Francisco, 2002).

[51] J. Bunch and M. Dunn, Solid State Commun. **152**, 1359 (2012).

[52] S. P. Koenig, N. Boddeti, M. L. Dunn, and J. S. Bunch, Nat. Nanotechnol. **6**, 543 (2011).

[53] W. H. Press, S. A. Teukolsky, W. T. Vetterling, and B. P. Flannery, *Numerical Recipes 3rd Edition: The Art of Scientific Computing* (Cambridge University Press, Cambridge, UK, 2007), pp. 597–600.

[54] M. Géradin and D. Rixen, *Mechanical Vibration: Theory and Application to Structural Dynamics* (Wiley, New York, 2014).

[55] Q. Lu, M. Arroyo, and R. Huang, J. Phys. D: Appl. Phys. **42**, 102002 (2009).

[56] Y. Wei, B. Wang, J. Wu, R. Yang, and M. L. Dunn, Nano Lett. **13**, 26 (2013).

[57] W. E. Arnoldi, Quart. Appl. Math. **9**, 17 (1951).

[58] M. K. Kadalbajoo and A. Gupta, Neural, Parallel Sci. Comput. **19**, 129 (2011).

[59] J. Chaste, M. Sledzinska, M. Zdrojek, J. Moser, and A. Bachtold, Appl. Phys. Lett. **99**, 213502 (2011).

[60] C. Si, Z. Liu, W. Duan, and F. Liu, Phys. Rev. Lett. **111**, 196802 (2013).

[61] E. V. Castro, H. Ochoa, M. I. Katsnelson, R. V. Gorbachev, D. C. Elias, K. S. Novoselov, A. K. Geim, and F. Guinea, Phys. Rev. Lett. **105**, 266601 (2010).